

Article

Climate Warming Benefits Plant Growth but Not Net Carbon Uptake: Simulation of Alaska Tundra and Needle Leaf Forest Using LPJ-GUESS

Cui Liu ¹, Chuanhua Li ^{1,2,*}  and Liangliang Li ¹

¹ College of Geography and Environmental Science, Northwest Normal University, Lanzhou 730070, China; lc1733133929@163.com (C.L.); allenecar@163.com (L.L.)

² Cryosphere Research Station on the Qinghai-Tibet Plateau, State Key Laboratory of Cryospheric Science, Northwest Institute of Eco-Environment and Resources, Chinese Academy of Sciences, Lanzhou 730000, China

* Correspondence: lch_nwnu@126.com

Abstract: Climate warming significantly impacts Arctic vegetation, yet its future role as a carbon sink or source is unclear. We analyzed vegetation growth and carbon exchange in Alaska's tundra and needle leaf forests using the LPJ-GUESS model. The accuracy of the model is verified using linear regression of the measured data from 2004 to 2008, and the results are significantly correlated, which proves that the model is reliable, with R^2 values of 0.51 and 0.46, respectively, for net ecosystem carbon exchange (NEE) at the tundra and needle leaf forest sites, and RMSE values of 22.85 and 23.40 $\text{gC}/\text{m}^2/\text{yr}$ for the tundra and needle forest sites, respectively. For the gross primary production (GPP), the R^2 values were 0.66 and 0.85, and the RMSE values were 39.25 and 43.75 $\text{gC}/\text{m}^2/\text{yr}$ at the tundra and needle leaf forest sites, respectively. We simulated vegetation carbon exchanges for 1992–2014 and projected future exchanges for 2020–2100 using climate variables. Under SSP1-2.6, SSP2-4.5, and SSP5-8.5 scenarios, GPP values increase with higher emissions, while the NEE showed great fluctuations without significant differences among the three pathways. Our results showed although climate warming can benefit vegetation growth, net carbon assimilation by vegetation may not increase accordingly in the future.

Keywords: climate warming; carbon uptake; LPJ-GUESS; Alaska tundra



Citation: Liu, C.; Li, C.; Li, L. Climate Warming Benefits Plant Growth but Not Net Carbon Uptake: Simulation of Alaska Tundra and Needle Leaf Forest Using LPJ-GUESS. *Land* **2024**, *13*, 632. <https://doi.org/10.3390/land13050632>

Academic Editors: Baojie He, Siliang Yang, K. Venkatachalam and Amos Darko

Received: 21 March 2024

Revised: 1 May 2024

Accepted: 4 May 2024

Published: 8 May 2024



Copyright: © 2024 by the authors. Licensee MDPI, Basel, Switzerland. This article is an open access article distributed under the terms and conditions of the Creative Commons Attribution (CC BY) license (<https://creativecommons.org/licenses/by/4.0/>).

1. Introduction

From 2011 to 2020, the global surface temperature increased by 1.09 °C compared to the period from 1850 to 1900 [1]. This warming rate was about 50% faster in the United States and two to three times faster across the Eurasian continent, while the Arctic and Antarctic Peninsula experienced warming rates three to four times greater [2]. Additionally, significant changes in the hydrological cycle, such as precipitation and evapotranspiration, were observed in high-latitude regions [3]. Climate change has led to widespread alterations and successions in biological communities, with alpine forest–tundra ecotones shifting to higher elevations, deciduous and boreal forests moving toward polar regions, an increase in woody vegetation in subarctic tundra, and a significant reduction in global grassland areas. In temperate and polar zones, approximately half of treelines are shifting toward the poles or higher altitudes, and alpine meadows are decreasing [4]. Climate warming has advanced the spring phenological phases of species in temperate regions and has also enhanced rice and corn yields in the Kosy River Basin [5]. These changes in vegetation composition and productivity in high-latitude areas are further impacting the global carbon cycle [6,7].

Arctic ecosystems have long been exposed to low temperatures and are highly vulnerable to climate change [8,9]. According to the definition of the Arctic Monitoring and

Assessment Programme (AMAP) [10], the Arctic land area accounts for 5.37% of the world's land area, and the vegetative area in the Arctic is 71.02% [11]. Vegetation changes in this region play an important role in regulating the global carbon balance because the vast areas in this region belong to permafrost zones, where the soil organic carbon content is high [12–14]. The changes in vegetation dynamics and species compositions in the Arctic have attracted many concerns. However, there are still great uncertainties in the net ecosystem carbon exchanges in this region due to the lack of long-term observational data [15,16].

Vegetation is an important component of the global carbon cycle. Carbon assimilation by vegetation plays a key role in determining the roles of the ecosystem as a carbon source or sink [17]. Vegetation type shifts, particularly shrub expansion across the Arctic tundra, have been widely regarded as a result of rapid climate warming [18,19]. The changes in vegetation can also potentially alter ecosystem carbon balances by affecting interactions among the soil–plant–atmosphere [20]. Presently, process models have been widely used to study vegetation growth and the carbon cycle in terrestrial ecosystems [20,21]. For example, based on in situ observation data, ecological process-based models can assess how the carbon balance will be impacted by climate change in Arctic tundra ecosystems [22]. Among these models, the LPJ-GUESS (Lund–Potsdam–Jena general ecosystem simulator) is a coupled biogeochemical model that has a wide range of applications in vegetation productivity estimation and vegetation carbon cycle under the current and future climate scenarios [21,23–27].

The purpose of this study is twofold. First, to explore the trends in vegetation GPP and carbon budget changes in the tundra and boreal forest ecosystems of Alaska from 1992 to 2014. Second, to analyze whether future reliance on vegetation to absorb more carbon is feasible by simulating the trends in vegetation GPP and carbon budget changes for the two aforementioned ecosystems under three future climate scenarios. To address these scientific inquiries, this study rigorously validates the LPJ-GUESS model using field monitoring data spanning 4 to 5 years to ensure its accuracy in simulating carbon cycling during historical periods. Subsequently, detailed simulations of vegetation carbon budgets from 1992 to 2014 are conducted, extending further to predictive analyses under future climatic conditions. These research findings offer crucial insights into understanding the growth dynamics of Arctic vegetation amidst climate change and its potential contribution to the global carbon cycle. They also provide scientific grounds for assessing the possibility of future vegetation GPP as a carbon sink.

2. Materials and Methods

2.1. Study Area

The land cover types in Alaska are dominated by forests and tundra [28]. Accordingly, we select two sites as representatives of the two land cover types in this area (Figure 1). One site is the tundra ecosystem, e.g., Atqasuk, with the site name US-ATQ (70.47° N, 157.41° W). The elevation is 15 m above sea level. From 1989 to 2014, the average annual temperature is -9.7 °C, and the average annual precipitation is 93 mm. The vegetation communities at this site are dominated by sedges, grasses, mosses, and dwarf shrubs (<40 cm). The ATQ site belongs to the continuous permafrost region with high ground ice content. The other is the needle leaf forest site, e.g., the Poker Flat Research Range Black Spruce Forest, with the site name of US-PRR (65.12° N, 147.48° W). The elevation is 210 m above the site level. At the US-PRR site, the average annual temperature is -2 °C, and the average annual precipitation is 275 mm. The land cover type belongs to the evergreen needle leaf (ENF), and this area is covered with extensive forest. The PRR site belongs to discontinuous permafrost regions with medium ground ice content.

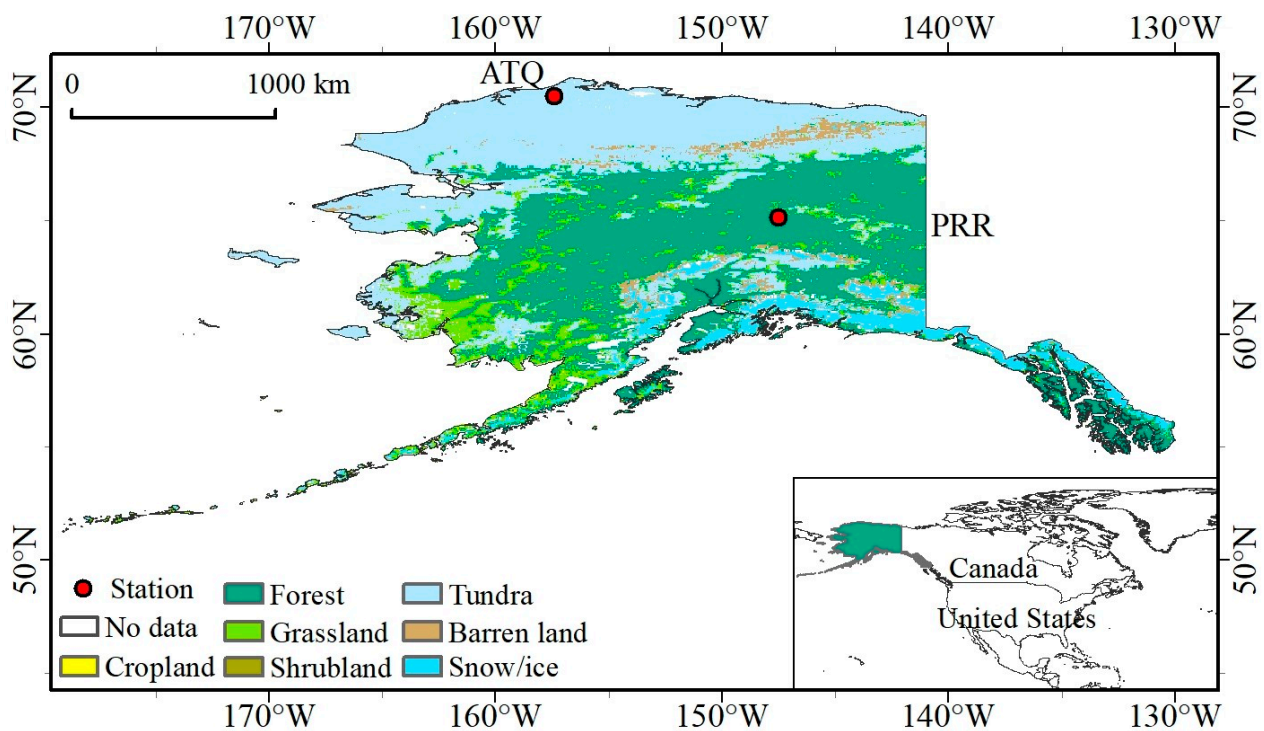


Figure 1. Location of the sites and the land cover types in Alaska. Alaska boundary data were downloaded from the website (https://gadm.org/download_country_v3.html, accessed on 12 April 2023). Land cover data were downloaded from the website <https://doi.pangaea.de/10.1594/PANGAEA.913496>, accessed on 12 April 2023.

2.2. Data

The climate data for the ATQ tundra and the PRR needle leaf forest sites (1992–2014), including the monthly precipitation, monthly air temperatures, monthly solar radiation, and annual atmospheric carbon dioxide concentrations, were downloaded from the website (<https://fluxnet.org/data/download-data/>, accessed on 14 April 2023). Validation data for gross primary production (GPP) and net ecosystem exchanges (NEE) were obtained from FLUXNET2015 (Supporting Information Text S1). There were two different time periods for the two sites, e.g., 2004–2008 for the ATQ site and 2011–2014 for the PRR site were downloaded from the website (<https://fluxnet.org/data/fluxnet2015-dataset/>, accessed on 12 April 2023). We selected the NEE and NPP data to assess the model accuracy.

We selected three scenario datasets from the CMIP6 SSP1-2.6, SSP2-4.5, and SSP5-8.5: the SSP1-2.6 “2 °C scenario” of the “sustainability” SSP1 socio-economic family, whose nameplate 2100 radiative forcing level is 2.6 W m^{-2} ; the SSP2-4.5 of the “middle of the road” socio-economic family SSP2 with a nominal 4.5 W m^{-2} radiative forcing level by 2100; and the SSP5-8.5 marks the upper edge of the SSP scenario spectrum with a high reference scenario in a high fossil-fuel development world throughout the 21st century. The precipitation, temperature, solar radiation, carbon dioxide, gross primary production, and leaf area index in the three pathways were downloaded (<https://esgf-node.llnl.gov/search/cmip6/>, accessed on 14 April 2023) (Supporting Information Text S2). The detailed description of the data is shown in Tables 1 and 2. We converted units of air temperature from Kelvin to Celsius, units of precipitation are mm year^{-1} , and units of GPP from $\text{kgC m}^{-2} \text{ s}^{-1}$ to $\text{gC m}^{-2} \text{ yr}^{-1}$. The changing trends of precipitation (Figure 2), temperature (Figure 3), solar radiation (Figure 4), and carbon dioxide concentration at the ATQ tundra and PRR needle leaf forest sites from 2020 to 2100 are shown in Figures 2–4.

Table 1. SSP scenario data required by the model.

Variable	Name (Unit)	Pathway	Model
CO ₂	Mole Fraction of CO ₂ (mol mol ⁻¹)	SSP126	NorESM2-LM
		SSP245	NorESM2-MM
		SSP585	NorESM2-MM
Pr	Precipitation (mm year ⁻¹)	SSP126	UKESM1-0-LL
		SSP245	UKESM1-0-LL
		SSP585	UKESM1-0-LL
Ta	Air Temperature (K)	SSP126	UKESM1-0-LL
		SSP245	UKESM1-0-LL
		SSP585	UKESM1-0-LL
Rss	Net Shortwave Surface Radiation (W m ⁻²)	SSP126	ACCESS-ESM1-5
		SSP245	ACCESS-ESM1-5
		SSP585	ACCESS-ESM1-5

Table 2. SSP scenario data required for the model comparison.

Variable	Name (Unit)	Pathway	Model
GPP	Carbon Mass Flux out of Atmosphere Due to Gross Primary Production on Land (kgC m ⁻² s ⁻¹)	SSP126	ACCESS-ESM1-5
		SSP245	ACCESS-ESM1-5
		SSP585	ACCESS-ESM1-5
LAI	Leaf Area Index (1)	SSP126	ACCESS-ESM1-5
		SSP245	ACCESS-ESM1-5
		SSP585	ACCESS-ESM1-5

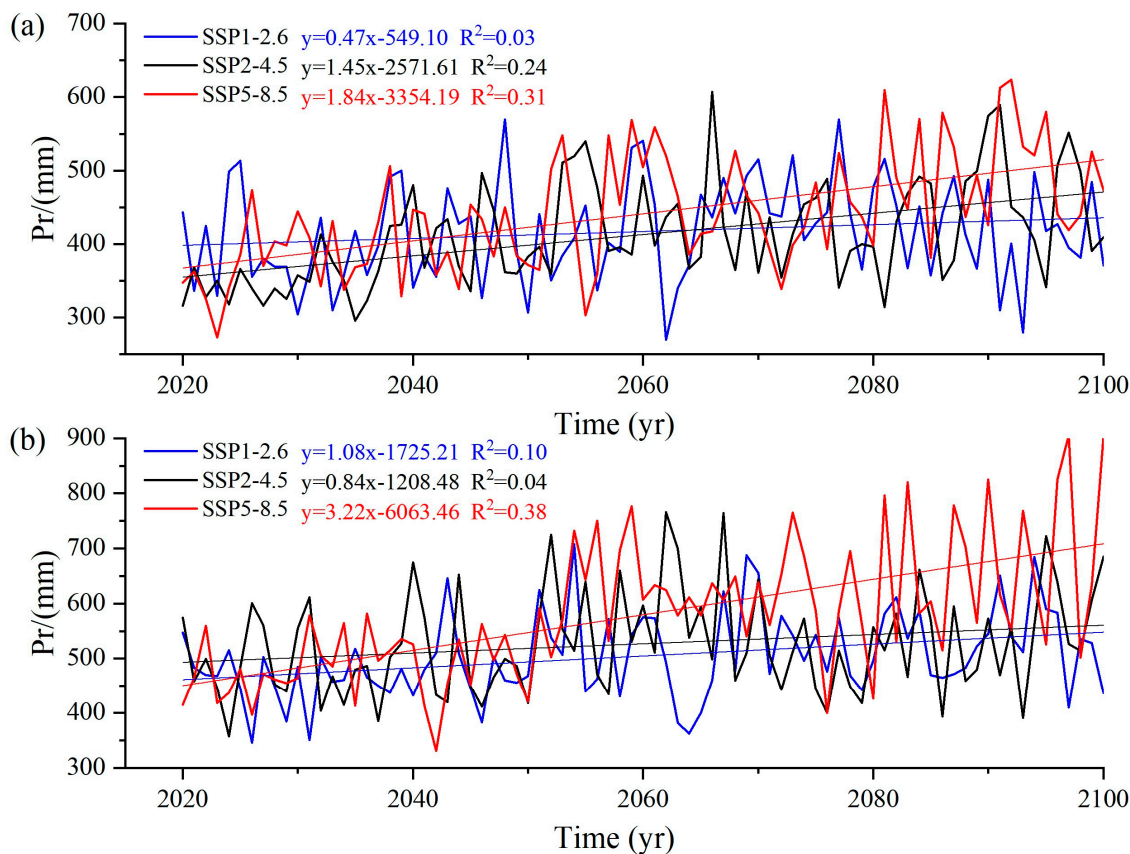


Figure 2. Precipitation changes in the future at the ATQ tundra site (a) and PRR needle leaf forest site (b).

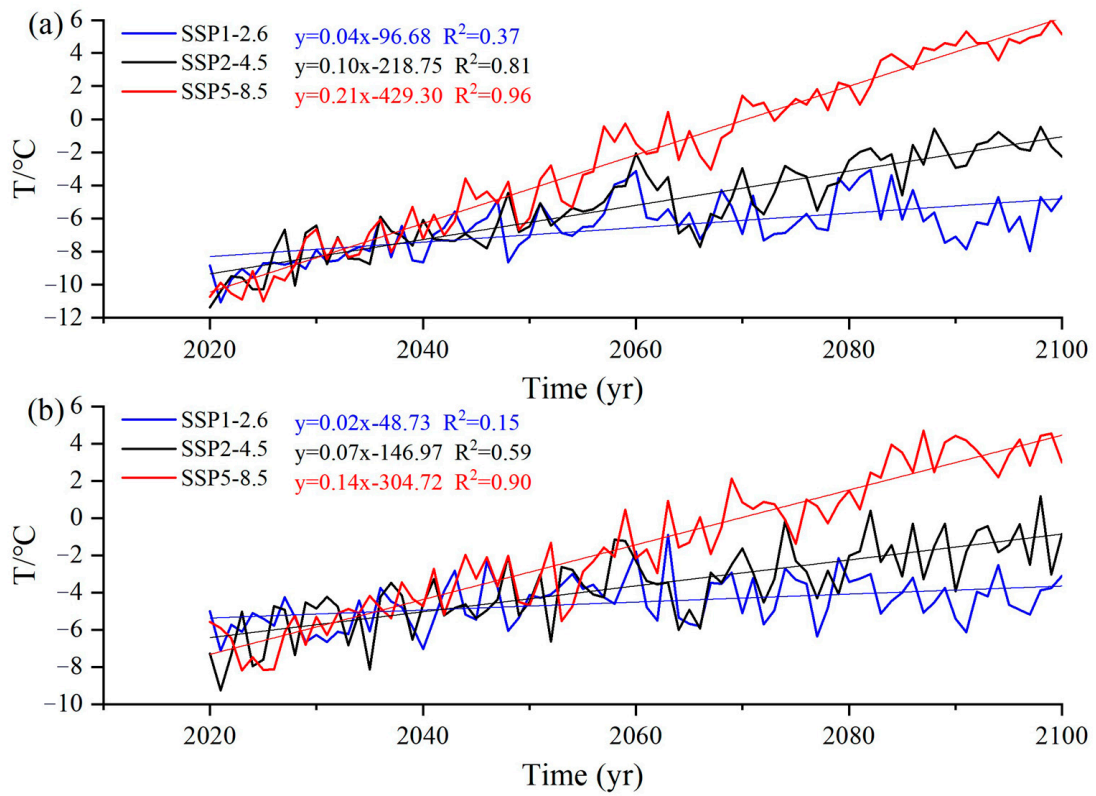


Figure 3. Temperature changes in the future at the ATQ tundra site (a) and PRR needle leaf forest site (b).

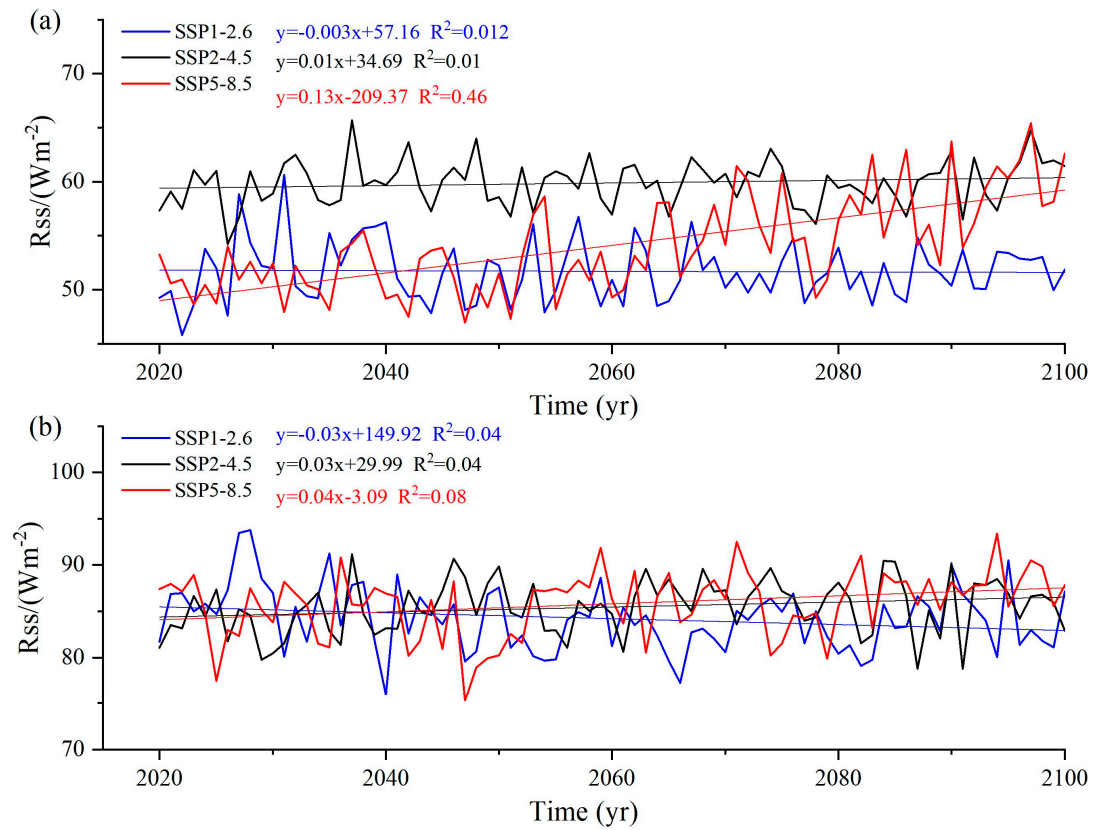


Figure 4. Solar radiation changes in the future at the ATQ tundra site (a) and PRR needle leaf forest site (b).

2.3. The LPJ-GUESS Model

The Lund–Potsdam–Jena general ecosystem simulator (LPJ-GUESS model) is developed based on the dynamic global vegetation model (LPJ-DGVM model), which combines the generalized physiological and biological processes in the LPJ-DGVM with representations of the tree population, demography, and canopy structures [29]. The LPJ-GUESS model combines terrestrial vegetation dynamics and land–atmosphere–carbon–water exchanges in a modular framework [30]. The model can simulate vegetation dynamics and carbon and water fluxes at species, communities, ecosystems, and even global scales. This model can predict vegetation changes under future climate scenarios [24], and it has been successfully used for modeling vegetation structure and biomass around the world [31,32]. The model simulates soil freeze–thaw processes and is suitable for the studies of processes at northern high latitudes. Therefore, we used it to study the future vegetation change in the Arctic ecosystem.

The LPJ-GUESS 4.1 version considers the soil freeze–thaw process and therefore performs well over the high latitudes in the north [31]. The data required to drive the model include monthly meteorological data (monthly temperature, monthly precipitation, and monthly solar radiation), annual atmospheric CO₂ concentration, and soil texture. The soil texture data applied in the LPJ-GUESS model were the soil dataset from the Food and Agriculture Organization of the United Nations (FAO) [33]. The soil type code is extracted from the file that comes with the model based on the geographic coordinates of the simulated points. In this model, vegetation is defined as a competing set of plant functional types (PFTs), grouped by similar attributes such as phenology, growth, life history, and bioclimatic constraints. The vegetation functional types used in this study consisted of three tree PFTs, a boreal needle-leaved evergreen tolerant tree (BNE), a boreal needle-leaved evergreen intolerant tree (BINE), and a broad-leaved evergreen intolerant tree (IBS), and a generic herbaceous PFT, grass (C3G) (Table 3). For the vegetation growth and carbon exchange simulation [34], the main output variables used in this study included the leaf area index (LAI), carbon biomass (C biomass), net primary production of ecosystems (NPP), net ecosystem exchange (NEE), and gross primary production of ecosystems (GPP).

Table 3. Plant functional types used in this study.

PFT	Distribution	Growth Form	Leaf Phenology	Shade-Tolerance	Photosynthetic Pathway
BNE	Boreal	Needle-leaved tree	Evergreen	Tolerant	C3
BINE	Boreal	Needle-leaved tree	Evergreen	Intolerant	C3
IBS	Boreal/temperate	Broad-leaved tree	Summer-green	Intolerant	C3
C3G	Boreal/temperate	Grass	Summer-green/rain-green	Intolerant	C3

In this study, climate data from 1989 to 2014 were used as input data for spin-up to repeatedly simulate the 200-year spin cycle and establish the equilibrium state of vegetation (Table 4). The input data of the model are SSP scenario data, such as temperature, precipitation, solar radiation, and carbon dioxide concentration, with a spatial resolution of 250 km. The vegetation conditions of the Arctic sites, such as the ATQ site and PRR site under SSP1-2.6, SSP2-4.5, and SSP5-8.5 scenarios in the future are simulated correspondingly.

Table 4. Parameter values in LPJ-GUESS Model.

Parameter	Parameter Value
vegmode	cohort
nyear_spinup	200
npatch	25
patcharea	1000

3. Results

3.1. Model Validation

The linear regressions showed that there were significant correlations between the simulated and observed values for NEE and GPP (Figure 5), indicating that the accuracy of the model was good. Therefore, it is possible to simulate the changes in NEE and GPP in this area under future climate conditions.

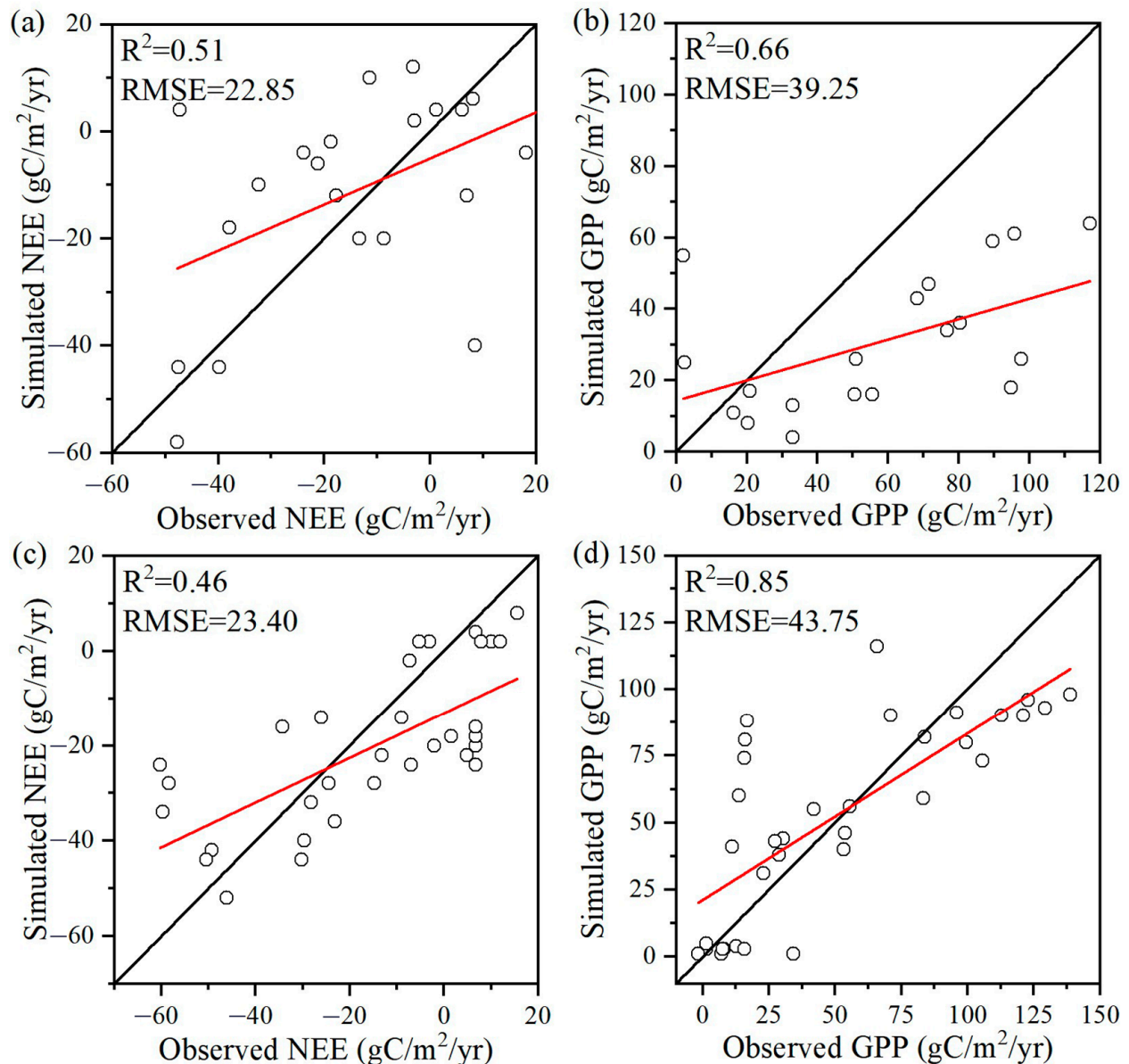


Figure 5. Simulated and observed NEE and GPP at the ATQ tundra site (a,b) and PRR needle leaf forest site (c,d).

The R^2 values of NEE at the tundra and needle leaf forest sites in Alaska were approximately 0.5, and the RMSE values were approximately 20 gC/m²/yr. The R^2 values of GPP at the tundra and needle leaf forest sites in Alaska were 0.66 and 0.85, respectively, and the RMSE values were 39.25 and 43.75 gC/m²/yr, respectively (Figure 5). This simulation accuracy was largely comparable with previous reports to the LPJ-GUESS. For example, the R^2 value of GPP in the Hindu Kush Himalayan forest simulated using LPJ-GUESS was 0.54 [26]. The R^2 value was 0.76 for the NEE simulation using a model of net CO₂ exchange in the Arctic tundra ecosystem from 2003 to 2009 [35]. Our results showed that

the LPJ-GUESS model is a useful tool to simulate NEE and GPP in the Arctic tundra and needle leaf forest.

3.2. NEE and GPP Simulation during 1992–2014

There are clear seasonal changes in NEE and GPP (Figure 6). During December–March, vegetation was dormant, and the NEE values showed that the ecosystems in the tundra and needle leaf forest sites were weak carbon sources. From May to August, the GPP at the tundra site was lower than that at the needle leaf forest site. The needle leaf forest was also a stronger carbon sink than the tundra.

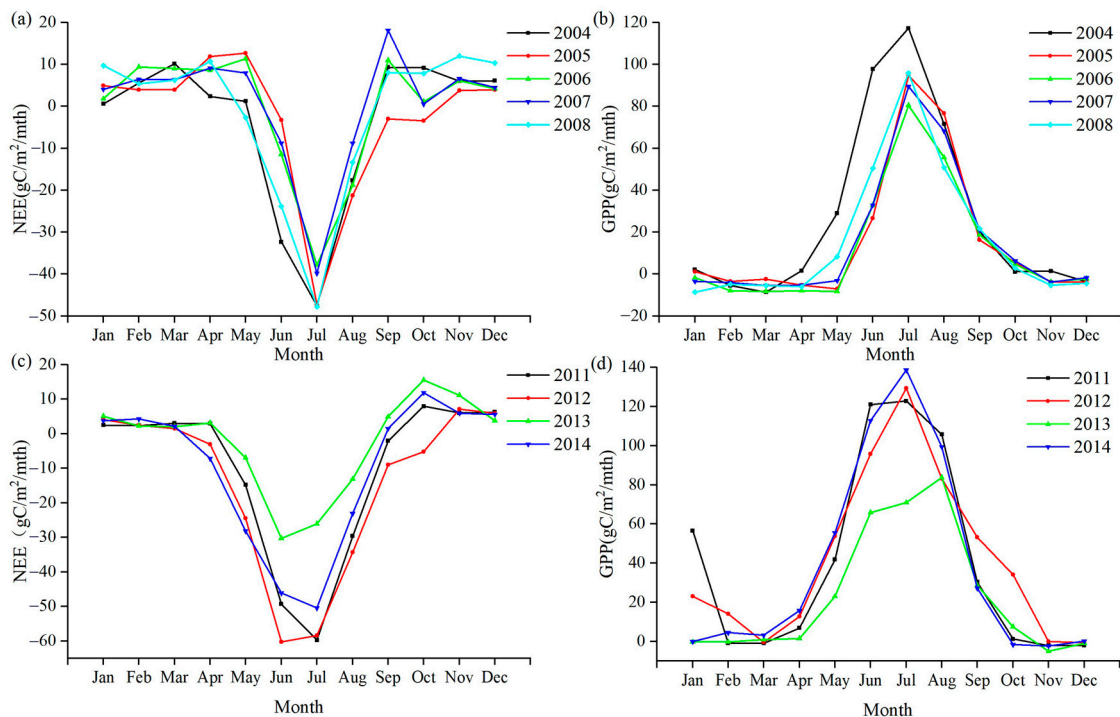


Figure 6. Monthly values of NEE and GPP values at the ATQ tundra site (a,b) and PRR needle leaf forest site (c,d).

The simulation results from 1992 to 2014 showed that the NEE values of the tundra site ranged from -123 to $8 \text{ gC/m}^2/\text{yr}$, with an average value of $-43.65 \text{ gC/m}^2/\text{yr}$ (Figure 7). The GPP values in the tundra forest ranged from 56 to $255 \text{ gC/m}^2/\text{yr}$, with an average value of $129 \text{ gC/m}^2/\text{yr}$. For the needle leaf forest, the average values of NEE and GPP were $-65 \text{ gC/m}^2/\text{yr}$ and $299 \text{ gC/m}^2/\text{yr}$, respectively.

3.3. Future Simulation of GPP and NEE

The simulation results of ATQ and PRR sites in the Arctic ecosystem have different results under the three future scenarios. Under future climate conditions, both the GPP at the tundra and needle leaf forest sites showed increasing trends (Figure 8). The average GPP values from 2020 to 2100 at the tundra site under SSP1-2.6, SSP2-4.5, and SSP5-8.5 were 22 , 31 , and $40 \text{ gC/m}^2/\text{yr}$, respectively. The average GPP values from 2020 to 2100 at the needle leaf forest site under the three pathways were 651 , 574 , and $831 \text{ gC/m}^2/\text{yr}$. For the NEE values, the tundra sites from 2020 to 2100 under SSP1-2.6, SSP2-4.5, and SSP5-8.5 were -36 , -43 , and $-48 \text{ gC/m}^2/\text{yr}$, respectively. The average NEE values at the needle leaf forest site from 2020 to 2100 were -229 , -226 , and $-276 \text{ gC/m}^2/\text{yr}$, respectively (Figure 8). The rate of decline of NEE at the ATQ tundra site was the fastest under the SSP5-8.5 pathway from 2020 to 2100. For the PRR needle leaf forest site, the carbon uptake rate was the fastest under the SSP1-2.6 pathway, followed by SSP5-8.5. For the GPP values,

both the ATQ tundra site and PRR needle leaf forest site had the greatest increasing value under the SSP5-8.5 pathway.

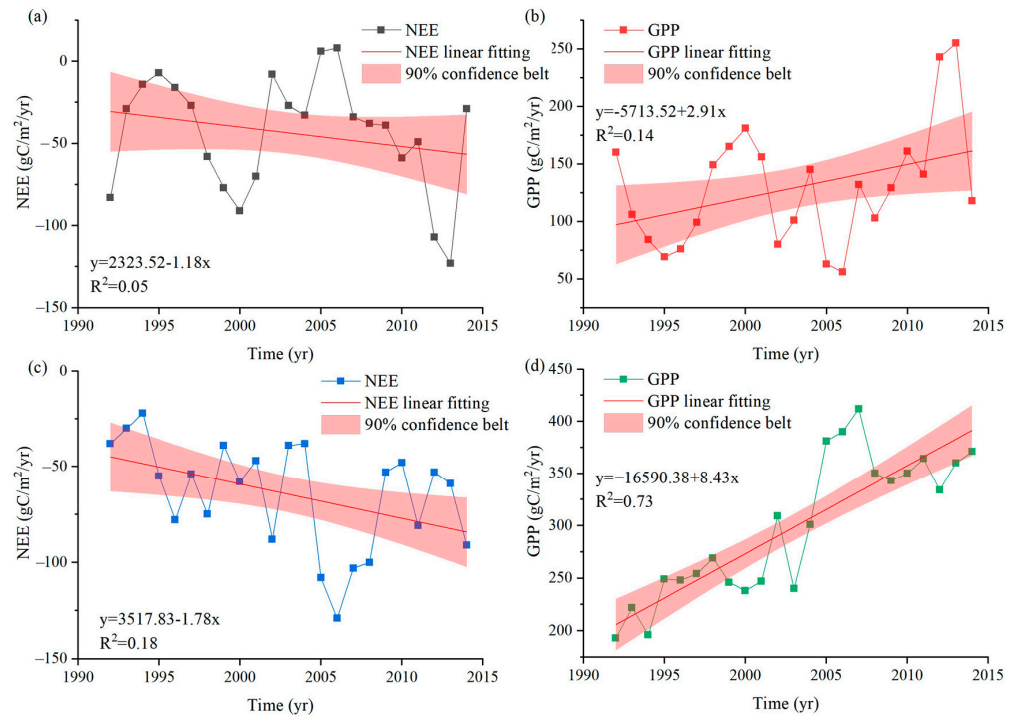


Figure 7. Changes in NEE and GPP from 1992 to 2014 at the ATQ tundra (a,b) and PRR needle leaf forest (c,d) sites.

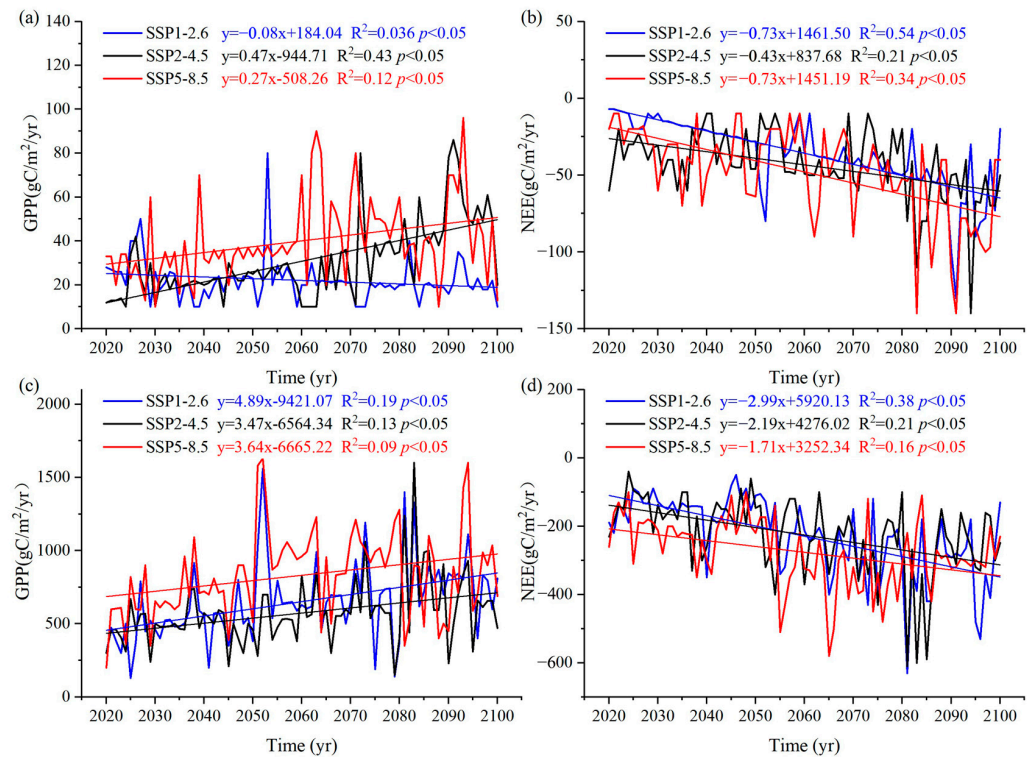


Figure 8. Changes in GPP and NEE from 2020 to 2100 under future climate conditions at the ATQ tundra site (a,b) and PRR needle leaf forest site (c,d).

The carbon exchange of the Arctic ecosystem in a future climate is simulated (Table 5). In the future scenario, the carbon exchange of the PRR site is higher than that of the ATQ site, in which the SSP5-8.5 pathway is higher than that of the SSP1-2.6 pathway, but the transformation rate of the SSP1-2.6 pathway is faster than that of SSP5-8.5 pathway. The net vegetation carbon exchange rate was higher than the net soil carbon exchange rate.

Table 5. Future simulation of carbon exchange.

Site	Climate Scenarios	Carbon Exchange (gC/m ² /yr)			Rate of Change (gC/m ² /yr ²)		
		NEE	Veg.	Soil	NEE	Veg.	Soil
ATQ	SSP1-2.6	−36.00	−45.00	16.03	−0.73	−3.59	0.41
	SSP2-4.5	−43.00	−115.33	40.98	−0.43	−3.00	0.45
	SSP5-8.5	−48.00	−113.11	53.90	−0.73	−0.27	0.91
PRR	SSP1-2.6	−229.00	−348.71	282.93	−2.99	−2.89	2.27
	SSP2-4.5	−226.00	−298.55	231.98	−2.19	−2.12	1.29
	SSP5-8.5	−276.00	−454.78	361.36	−1.71	−1.13	2.61

3.4. Comparison of GPP and LAI Simulation Results

We compared the simulated GPP and LAI values from LPJ-GUESS model, and the GPP and LAI values of the ESM output (Figures 9 and 10). We found that in the GPP simulation, the PRR site fits the ESM output value better than the ATQ site, and the simulated value of the ATQ site is lower than the ESM output value, while the simulated value of the PRR site is higher than the ESM output value. For LAI simulation, the ATQ site fitting degree was higher than that of the PRR site, the model fitting value of the PRR site was generally lower than that of the ATQ site, and the model simulation value had periodic fluctuations.

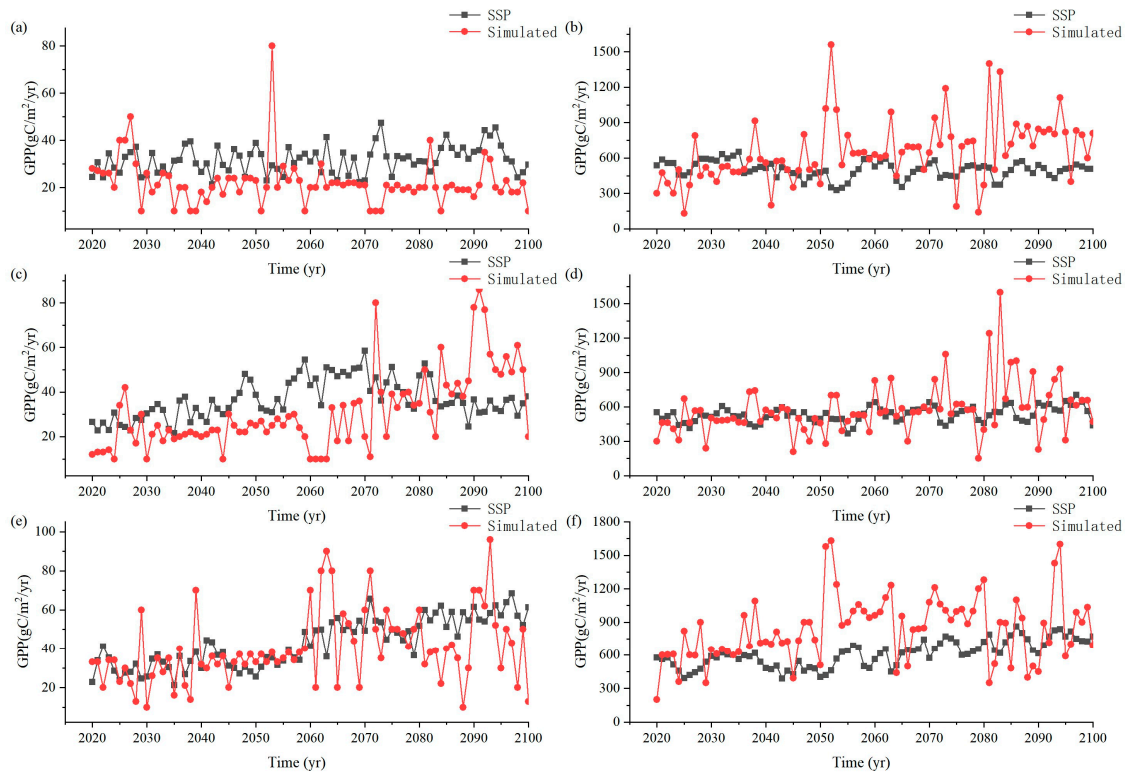


Figure 9. Comparison of GPP values between model simulation and ESM output at the ATQ tundra site ((a) (SSP1-2.6), (c) (SSP2-4.5), (e) (SSP5-8.5)) and PRR needle leaf forest site ((b) (SSP1-2.6), (d) (SSP2-4.5), (f) (SSP5-8.5)) in SSP scenario.

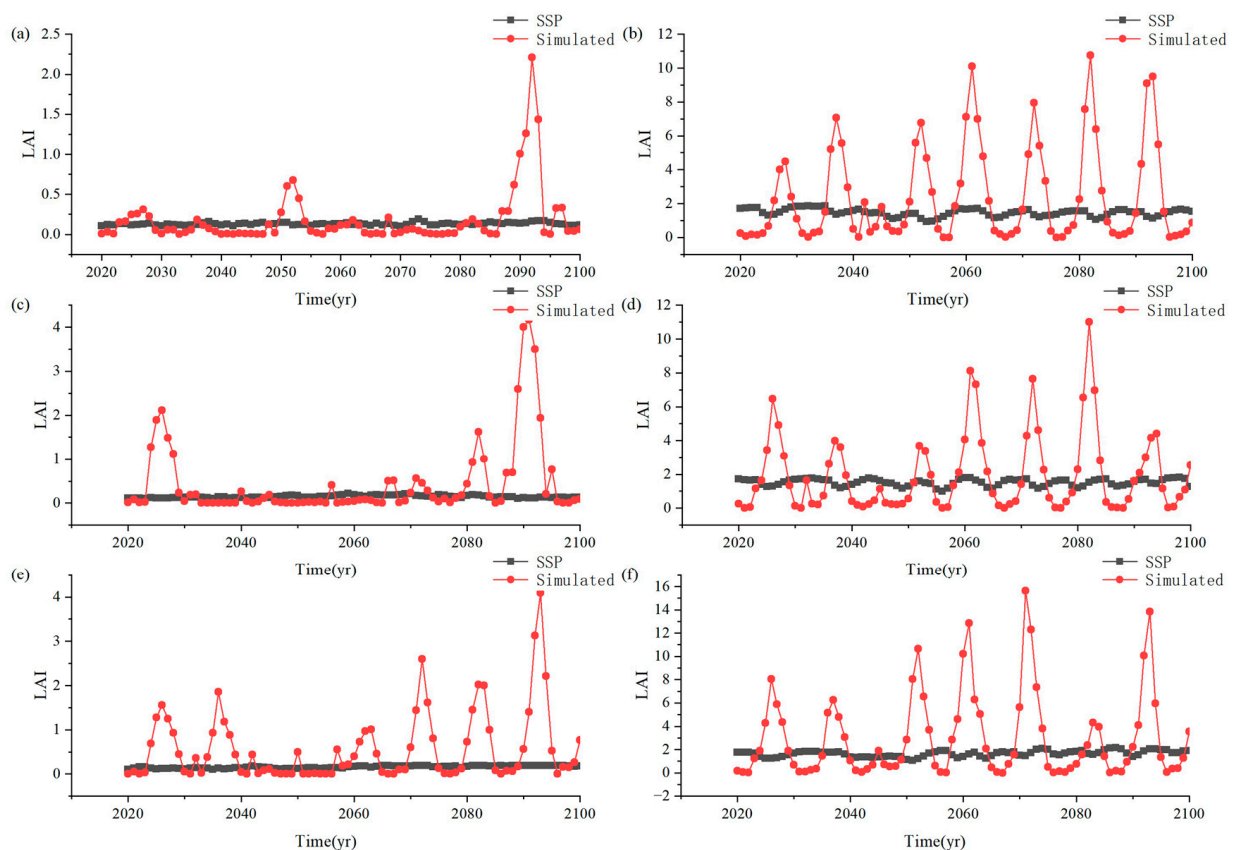


Figure 10. Comparison of LAI value between model simulation and ESM output at the ATQ tundra site ((a) (SSP1-2.6), (c) (SSP2-4.5), (e) (SSP5-8.5)) and PRR needle leaf forest site ((b) (SSP1-2.6), (d) (SSP2-4.5), (f) (SSP5-8.5)) in SSP scenario.

4. Discussion

4.1. Model Simulation Values

The LPJ-GUESS model has been widely used to estimate the impacts of climate on terrestrial ecosystems [36–39]. In light of this, our study simulated NEE and GPP using the LPJ-GUESS model, achieving a level of accuracy comparable to previous research reports, thereby ensuring the reliability of our results [26]. The NEE and GPP in our study area showed obvious seasonal changes (Figure 6). It is reasonable that the NEE values are negative during the growing season because vegetation growth can assimilate carbon [40]. The maximum carbon assimilation rates largely occurred in July or August because during this period, the air temperature was high, and the solar radiation was strong in the Arctic region. From April to July, the GPP values also increase rapidly, and this pattern clearly demonstrates the seasonal changes in vegetation growth. In the tundra ecosystem, GPP began to increase from early to mid-June and peaked from late July to early August. After the peak values in summer, GPP began to decline. In the tundra ecosystem, the seasonality of ecosystem respiration was less obvious [41]. Thus, the seasonality of NEE was determined by GPP rather than ecosystem respiration in tundra ecosystems. Compared with the tundra, GPP and ecosystem respiration in boreal forest ecosystems show similar seasonality, peaking between late June and mid-July. Although the specific peak times of GPP and NEE vary from site to site, they show similar seasonal variation [42].

Our simulation results showed that the NEE at the needle leaf forest site was lower than that of the tundra, indicating that the needle leaf forest is a stronger carbon sink during the growing season. Similarly, the GPP of the needle leaf forest site was higher than that of the tundra site (Figure 5). Compared with tundra ecosystems, forest ecosystems have richer biodiversity, more complex structural levels, and higher productivity, and their annual

carbon sequestration capacity is higher [43]. Fisher et al. showed a comparison of NEE and GPP simulations using 10 NACP site synthesis models in 2002 and 2003 in Alaska tundra sites. NEE reached its lowest value, and GPP reached its highest value around July and gradually approached zero in winter. The terrestrial biosphere model was used for the simulation; GPP was $220 \pm 500 \text{ gC/m}^2/\text{yr}$, and NEE was $10 \pm 190 \text{ gC/m}^2/\text{yr}$, which were consistent with the results of this study [44].

4.2. Changes in NEE and GPP in Alaska from 1992 to 2014

From 1992 to 2014, NEE and GPP of ATQ sites showed a trend of drastic fluctuation, which was due to fire disturbance. The ecosystem was disturbed by fires during 1982–2002 and 2003–2011 at the ATQ site, which led to drastic changes in the carbon flux of the ecosystem [42]. At the beginning of the fire period (1982–1995), the disturbance of the ecosystem was remarkable. During this period, the fire led to a decrease in the flux and GPP showing a downward trend, with less GPP in burn sites than in uninterrupted areas [42].

With the decrease of GPP related to recent disturbances, NEE showed an overall trend of increasing. In the late period of the fire (1995–2002), the vegetation in the burned ecosystem began recovering slowly, and the GPP showed an upward trend while the NEE showed a downward trend [42]. The change trend of NEE and GPP of the PRR site was consistent during the same period, because they were not disturbed.

From 1992 to 2014, the decreasing NEE values indicated that the carbon uptake rates increased, and the GPP values also increased. Compared with the tundra site, the needle leaf forest site had a faster-increasing rate of carbon uptake and GPP values. Similar findings have also been reported by in situ observation data, i.e., the carbon uptake rates of forest regions have been increasing during the past decades, while the tundra areas showed little change in carbon uptake rates [45]. This can be attributed to the fact that the tundra area is dominated by herbaceous species, which have limited biomass and carbon uptake capacity. It has also been found that Arctic tundra may already be a carbon source because of limited vegetation growth but high soil organic carbon loss [46,47]. In addition, the NEE and GPP at the tundra sites showed greater fluctuations than those at the needle leaf forest site. This pattern confirmed that the growth of perennial herbs is more sensitive to climate conditions, while woody forests have a stronger adaptive capacity to climate conditions. Consequently, the GPP values for the forest usually showed smaller changes than those in grassland [48].

4.3. Simulations under Future Climate Scenarios

The simulation results show that from 2020 to 2100, the GPP values at both sites increased. The carbon uptake rates in tundra vary greatly under different climate scenarios. Climate warming at high latitudes can alleviate the effects of cold stress on vegetation growth [49] and thus promote vegetation growth [50]. With the increase in temperature, precipitation, and atmospheric CO_2 content, the Arctic will show a “greening” trend [51]. A previous study based on the CoupModel simulation in the Greater Khingan Mountains permafrost region also suggested that the GPP and carbon uptake tended to increase in a warming climate. We found that the maximum GPP values appeared under the SSP5-8.5 scenario, and the minimum values appeared under the SSP1-2.6 scenario. However, the carbon uptake rates showed much lower increasing rates. Under the SSP5-8.5 scenario, the GPP values are the highest, due to this prediction of higher greenhouse gas emissions and temperature rise, which typically enhances the growth rate and biomass of vegetation in certain regions, particularly in temperate and high-latitude areas [52]. In contrast, the SSP1-2.6 scenario forecasts more moderate greenhouse gas emissions and climate change, resulting in relatively lower GPP values. However, despite the increase in GPP under certain scenarios, the rate of carbon sequestration is relatively slow. This is partly the elevated concentrations of greenhouse gases and rising temperatures accelerate the thawing of permafrost. As permafrost thaws, the previously frozen organic is released and decomposed through microbial activity, promoting soil respiration [53,54]. Soil respiration,

the process by which soil microorganisms decompose organic matter and release carbon dioxide, is enhanced by these conditions, leading to the release of carbon from the soil into the atmosphere, thereby offsetting some of the carbon fixed by the increased photosynthesis due to vegetation growth [55]. In summary, while climate warming may promote vegetation growth and primary productivity in the short term, the accelerated thawing of permafrost and the increase in soil respiration could lead to a future where carbon sequestration in the Arctic region may not significantly increase.

In the future scenario, the NEE value simulated using the model shows a decreasing trend, which means that the carbon sequestration capacity of the ATQ tundra site and PRR needle leaf forest site in the Arctic region will increase, and the carbon sequestration capacity of PRR site will be stronger and the vegetation growth condition will be better. Under the future warming scenario, the net vegetation carbon exchange of tundra sites is larger than that of forest sites, while the net soil carbon exchange is smaller than that of forest sites. The decomposition of soil organic matter is positively correlated with soil temperature, and the net soil carbon exchange rate will accelerate with future temperature increases. In the Arctic ecosystem, the net soil carbon exchange rate of forest sites is greater than that of tundra sites. In the SSP1-2.6 scenario, the rate of carbon sequestration in coniferous forest sites is the fastest, likely reflecting the relatively mild climate conditions of this scenario that favor carbon fixation. Overall, the carbon exchange at PRR coniferous forest sites is higher than that at ATQ permafrost sites, possibly due to the greater biomass and carbon storage capacity of coniferous forests [56]. Although carbon exchange is higher under the SSP5-8.5 scenario than under SSP1-2.6, the transformation rate is quicker in the SSP1-2.6 scenario, indicating that ecosystems under scenarios with lower greenhouse gas emissions adapt and respond more rapidly to climate change.

We re-drive the model based on the SSP1-2.6 scenario, changing the driving factor one at a time, and changing the carbon dioxide concentration, air temperature, precipitation, and solar radiation to the corresponding factors of the SSP2-4.5 scenario and SSP5-8.5 scenario, respectively. The results show that in the GPP and NEE simulation results, carbon dioxide concentration has the largest effect, followed by air temperature and solar radiation, and precipitation has the least effect. The increase in air temperature, solar radiation, and precipitation has a positive effect on GPP in Alaska. This suggests that future improvements in hydrothermal conditions induced by climate change will alleviate temperature stress in Alaska and have a positive effect on improving ecosystem productivity (Supporting Information Text S3).

5. Conclusions

We discuss the impact of future climate on Arctic ecosystems by simulating vegetation growth at a tundra site and a forest site. In this study, we simulated the changing trends of NEE and GPP of the tundra and needle leaf forest in Alaska from 1992 to 2014 and their future changes by 2100 using the LPJ-GUESS model. Our results showed that the LPJ-GUESS model is a useful tool to simulate the NEE and GPP for these two land cover types. During the past decades, the GPP showed a faster-increasing rate in the needle leaf forest site than in the tundra site, and the carbon uptake rates for the two areas fluctuated considerably, with nonsignificant increasing trends. Under the future emission pathways, the GPP values of the tundra and needle leaf forest were also higher, while the carbon uptake showed no significant increasing trends in the future. Under the future emission pathways, the GPP of the high emission SSP5-8.5 scenario increases faster and NEE decreases faster. In this study, we utilized the LPJ-GUESS model to simulate vegetation growth and carbon exchange processes in Alaska. The model validation period was relatively short, spanning only from 2004 to 2008, which may not fully capture the impacts of long-term climate change on the vegetation ecosystems. Additionally, while LPJ-GUESS is a well-recognized ecological model, its structure and parameter settings may not entirely reflect the complexities of the world.

Supplementary Materials: The following supporting information can be downloaded at <https://www.mdpi.com/article/10.3390/land13050632/s1>, Text S1. The supporting information contains detailed information of FLUXNET data; Text S2. The supporting information contains detailed information of CMIP6 data; Text S3, The supporting information contains detailed information of Supplementary data; Figure S1. Relationships among GPP, NEE and CO₂ concentration, Precipitation, Solar radiation, and air temperature for ATQ tundra site under SSP2-4.5 (a,c) and SSP 5-8.5 (b,d); Figure S2. Relationships among GPP, NEE and CO₂ concentration, Precipitation, Solar radiation, and air temperature for PRR needle leaf forest site under SSP2-4.5 (a,c) and SSP 5-8.5 (b,d).

Author Contributions: C.L. (Chuanhua Li) is responsible for the design of the project, revision of the paper, and acquisition of funding; C.L. (Cui Liu) is responsible for the implementation of the project, analysis of data, and drafting of the manuscript; L.L. is responsible for the collection and analysis of data. All authors have read and agreed to the published version of the manuscript.

Funding: This work was supported by the National Natural Science Foundation of China grant 42161058.

Data Availability Statement: Land cover data were downloaded from the website Liu, Gong, Wang, Clinton, Bai and Liang [27] (<https://doi.pangaea.de/10.1594/PANGAEA.913496>, accessed on 12 April 2023). The climate data and validation data were downloaded from the website (<https://fluxnet.org/data/download-data/>, accessed on 12 April 2023). Precipitation changes in the future [dataset] (Figure 2), temperature changes in the future [dataset] (Figure 3), solar radiation changes in the future [dataset] (Figure 4), simulated and observed NEE and GPP [dataset] (Figure 5), monthly NEE and GPP [dataset] (Figure 6), changes in NEE and GPP from 1992 to 2014 [dataset] (Figure 7), Changes in NEE and GPP from 2020 to 2100 [dataset] (Figure 8) are available at Dryad Digital Repository via <https://doi.org/10.5061/dryad.m63xsj451>.

Conflicts of Interest: The authors declare no conflicts of interest.

References

1. Arias, P.A.; Bellouin, N.; Coppola, E.; Jones, R.G.; Krinner, G.; Marotzke, J.; Naik, V.; Palmer, M.D.; Plattner, G.-K.; Rogelj, J.; et al. 2021: Technical Summary. In *Climate Change 2021: The Physical Science Basis. Contribution of Working Group I to the Sixth Assessment Report of the Intergovernmental Panel on Climate Change*; Masson-Delmotte, V., Zhai, P., Pirani, A., Connors, S.L., Péan, C., Berger, S., Caud, N., Chen, Y., Goldfarb, L., Gomis, M.I., et al., Eds.; Cambridge University Press: Cambridge, UK, 2021.
2. Hansen, J.; Ruedy, R.; Sato, M.; Lo, K. Global Surface Temperature Change. *Rev. Geophys.* **2010**, *48*. [[CrossRef](#)]
3. Park, H.; Tanoue, M.; Sugimoto, A.; Ichiyanagi, K.; Iwahana, G.; Hiyama, T. Quantitative separation of precipitation and permafrost waters used for evapotranspiration in a boreal forest: A numerical study using tracer model. *J. Geophys. Res. Biogeosci.* **2021**, *126*, e2021JG006645. [[CrossRef](#)]
4. Parmesan, C.; Morecroft, M.D.; Trisurat, Y. *Climate Change 2022: Impacts, Adaptation and Vulnerability*; GIEC: Melbourne, Canada, 2022.
5. Kumar, S.; Narjary, B.; Vivekanand; Islam, A.; Yadav, R.; Kamra, S. Modeling climate change impact on groundwater and adaptation strategies for its sustainable management in the Karnal district of Northwest India. *Clim. Change* **2022**, *173*, 3. [[CrossRef](#)]
6. Bjorkman, A.D.; Criado, M.G.; Myers-Smith, I.H.; Ravolainen, V.; Jonsdottir, I.S.; Westergaard, K.B.; Lawler, J.P.; Aronsson, M.; Bennett, B.; Gardfjell, H.; et al. Status and trends in Arctic vegetation: Evidence from experimental warming and long-term monitoring. *Ambio* **2020**, *49*, 678–692. [[CrossRef](#)] [[PubMed](#)]
7. Bruhwiler, L.; Parmentier, F.-J.W.; Crill, P.; Leonard, M.; Palmer, P.I. The Arctic carbon cycle and its response to changing climate. *Curr. Clim. Change Rep.* **2021**, *7*, 14–34. [[CrossRef](#)]
8. Cohen, J.; Zhang, X.; Francis, J.; Jung, T.; Kwok, R.; Overland, J.; Ballinger, T.J.; Bhatt, U.S.; Chen, H.W.; Coumou, D.; et al. Divergent consensus on Arctic amplification influence on midlatitude severe winter weather. *Nat. Clim. Change* **2020**, *10*, 20–29. [[CrossRef](#)]
9. Vavrus, S.J.; Holland, M.M.; Jahn, A.; Bailey, D.A.; Blazey, B.A. Twenty-First-Century Arctic Climate Change in CCSM4. *J. Clim.* **2012**, *25*, 2696–2710. [[CrossRef](#)]
10. AMAP. *AMAP Assessment Report: Arctic Pollution Issues. Arctic Monitoring and Assessment Programme (AMAP)*; AMAP: Oslo, Norway, 1998; p xii+859 pp.
11. Raynolds, M.K.; Walker, D.A.; Balsler, A.; Bay, C.; Campbell, M.; Cherosov, M.M.; Daniels, F.J.A.; Eidesen, P.B.; Emiokhina, K.A.; Frost, G.V.; et al. A raster version of the Circumpolar Arctic Vegetation Map (CAVM). *Remote Sens. Environ.* **2019**, *232*, 111297. [[CrossRef](#)]
12. Epstein, H.E.; Myers-Smith, I.; Walker, D.A. Recent dynamics of arctic and sub-arctic vegetation. *Environ. Res. Lett.* **2013**, *8*, 015040. [[CrossRef](#)]

13. Pearson, R.G.; Phillips, S.J.; Loranty, M.M.; Beck, P.S.A.; Damoulas, T.; Knight, S.J.; Goetz, S.J. Shifts in Arctic vegetation and associated feedbacks under climate change. *Nat. Clim. Change* **2013**, *3*, 673–677. [[CrossRef](#)]
14. Ping, C.; Jastrow, J.; Jorgenson, M.; Michaelson, G.; Shur, Y. Permafrost soils and carbon cycling. *Soil* **2015**, *1*, 147–171. [[CrossRef](#)]
15. Natali, S.M.; Holdren, J.P.; Rogers, B.M.; Treharne, R.; Duffy, P.B.; Pomerance, R.; MacDonald, E. Permafrost carbon feedbacks threaten global climate goals. *Proc. Natl. Acad. Sci. USA* **2021**, *118*, e2100163118. [[CrossRef](#)]
16. Virkkala, A.M.; Natali, S.M.; Rogers, B.M.; Watts, J.D.; Savage, K.; Connon, S.J.; Mauritz, M.; Schuur, E.A.G.; Peter, D.; Minions, C.; et al. The ABCflux database: Arctic-Boreal CO₂ flux observations and ancillary information aggregated to monthly time steps across terrestrial ecosystems. *Earth Syst. Sci. Data* **2022**, *2022*, 179–208. [[CrossRef](#)]
17. Zhao, M.W.; Yue, T.X.; Zhao, N.; Sun, X.F.; Zhang, X.Y. Combining LPJ-GUESS and HASM to simulate the spatial distribution of forest vegetation carbon stock in China. *J. Geogr. Sci.* **2014**, *24*, 249–268. [[CrossRef](#)]
18. Mekonnen, Z.A.; Riley, W.J.; Berner, L.T.; Bouskill, N.J.; Torn, M.S.; Iwahana, G.; Breen, A.L.; Myers-Smith, I.H.; Criado, M.G.; Liu, Y. Arctic tundra shrubification: A review of mechanisms and impacts on ecosystem carbon balance. *Environ. Res. Lett.* **2021**, *16*, 053001. [[CrossRef](#)]
19. Zhang, W.; Miller, P.A.; Smith, B.; Wania, R.; Koenigk, T.; Döscher, R. Tundra shrubification and tree-line advance amplify arctic climate warming: Results from an individual-based dynamic vegetation model. *Environ. Res. Lett.* **2013**, *8*, 034023. [[CrossRef](#)]
20. Friedlingstein, P.; Jones, M.W.; O’Sullivan, M.; Andrew, R.M.; Bakker, D.C.E.; Hauck, J.; Le Quere, C.; Peters, G.P.; Peters, W.; Pongratz, J.; et al. Global Carbon Budget 2021. *Earth Syst. Sci. Data* **2022**, *14*, 1917–2005. [[CrossRef](#)]
21. Sallaba, F.; Lehsten, D.; Seaquist, J.; Sykes, M.T. A rapid NPP meta-model for current and future climate and CO₂ scenarios in Europe. *Ecol. Model* **2015**, *302*, 29–41. [[CrossRef](#)]
22. Uchida, M.; Muraoka, H.; Nakatsubo, T. Sensitivity analysis of ecosystem CO₂ exchange to climate change in High Arctic tundra using an ecological process-based model. *Polar Biol.* **2016**, *39*, 251–265. [[CrossRef](#)]
23. Chaudhary, N.; Westermann, S.; Lamba, S.; Shurpali, N.; Sannel, B.K.; Schurgers, G.; Miller, P.A.; Smith, B. Modelling past and future peatland carbon dynamics across the pan-Arctic. *Global Change Biol.* **2020**, *26*, 4119–4133. [[CrossRef](#)]
24. Lindeskog, M.; Smith, B.; Lagergren, F.; Sycheva, E.; Ficko, A.; Pretzsch, H.; Rammig, A. Accounting for forest management in the estimation of forest carbon balance using the dynamic vegetation model LPJ-GUESS (v4.0, r9710): Implementation and evaluation of simulations for Europe. *Geosci. Model Dev.* **2021**, *14*, 6071–6112. [[CrossRef](#)]
25. Miller, P.A.; Smith, B. Modelling Tundra Vegetation Response to Recent Arctic Warming. *Ambio* **2012**, *41*, 281–291. [[CrossRef](#)]
26. Usman, H.; Pugh, T.A.M.; Ahlstrom, A.; Baig, S. Climate change projections of terrestrial primary productivity over the Hindu Kush Himalayan forests. *Earth Syst. Dynam.* **2021**, *12*, 857–870. [[CrossRef](#)]
27. Smith, B.; Warlind, D.; Arneth, A.; Hickler, T.; Leadley, P.; Silberg, J.; Zaehle, S. Implications of incorporating N cycling and N limitations on primary production in an individual-based dynamic vegetation model. *Biogeosciences* **2014**, *11*, 2027–2054. [[CrossRef](#)]
28. Jin, S.; Yang, L.; Zhu, Z.; Homer, C. A land cover change detection and classification protocol for updating Alaska NLCD 2001 to 2011. *Remote Sens. Environ.* **2017**, *195*, 44–55. [[CrossRef](#)]
29. Hickler, T.; Vohland, K.; Feehan, J.; Miller, P.A.; Smith, B.; Costa, L.; Giesecke, T.; Fronzek, S.; Carter, T.R.; Cramer, W.; et al. Projecting the future distribution of European potential natural vegetation zones with a generalized, tree species-based dynamic vegetation model. *Glob. Ecol. Biogeogr.* **2012**, *21*, 50–63. [[CrossRef](#)]
30. Ekici, A.; Chadburn, S.; Chaudhary, N.; Hajdu, L.H.; Marmy, A.; Peng, S.; Boike, J.; Burke, E.; Friend, A.D.; Hauck, C.; et al. Site-level model intercomparison of high latitude and high altitude soil thermal dynamics in tundra and barren landscapes. *Cryosphere* **2015**, *9*, 1343–1361. [[CrossRef](#)]
31. Pongracz, A.; Warlind, D.; Miller, P.A.; Parmentier, F.J.W. Model simulations of arctic biogeochemistry and permafrost extent are highly sensitive to the implemented snow scheme in LPJ-GUESS. *Biogeosciences* **2021**, *18*, 5767–5787. [[CrossRef](#)]
32. Tang, J.; Pilesjo, P.; Miller, P.A.; Persson, A.; Yang, Z.L.; Hanna, E.; Callaghan, T.V. Incorporating topographic indices into dynamic ecosystem modelling using LPJ-GUESS. *Ecohydrology* **2014**, *7*, 1147–1162. [[CrossRef](#)]
33. Sun, G.D.; Mu, M. The analyses of the net primary production due to regional and seasonal temperature differences in eastern China using the LPJ model. *Ecol. Model* **2014**, *289*, 66–76. [[CrossRef](#)]
34. Gustafson, A.; Miller, P.A.; Bjork, R.G.; Olin, S.; Smith, B. Nitrogen restricts future sub-arctic treeline advance in an individual-based dynamic vegetation model. *Biogeosciences* **2021**, *18*, 6329–6347. [[CrossRef](#)]
35. Shaver, G.R.; Rastetter, E.B.; Salmon, V.; Street, L.E.; van de Weg, M.J.; Rocha, A.; van Wijk, M.T.; Williams, M. Pan-Arctic modelling of net ecosystem exchange of CO₂. *Philos. Trans. R. Soc. B* **2013**, *368*, 20120485. [[CrossRef](#)] [[PubMed](#)]
36. Morales, P.; Sykes, M.T.; Prentice, I.C.; Smith, P.; Smith, B.; Bugmann, H.; Zierl, B.; Friedlingstein, P.; Viovy, N.; Sabaté, S. Comparing and evaluating process-based ecosystem model predictions of carbon and water fluxes in major European forest biomes. *Glob. Change Biol.* **2005**, *11*, 2211–2233. [[CrossRef](#)] [[PubMed](#)]
37. Jung, M.; Le Maire, G.; Zaehle, S.; Luyssaert, S.; Vetter, M.; Churkina, G.; Ciais, P.; Viovy, N.; Reichstein, M. Assessing the ability of three land ecosystem models to simulate gross carbon uptake of forests from boreal to Mediterranean climate in Europe. *Biogeosciences* **2007**, *4*, 647–656. [[CrossRef](#)]
38. Sitch, S.; Smith, B.; Prentice, I.C.; Arneth, A.; Bondeau, A.; Cramer, W.; Kaplan, J.O.; Levis, S.; Lucht, W.; Sykes, M.T. Evaluation of ecosystem dynamics, plant geography and terrestrial carbon cycling in the LPJ dynamic global vegetation model. *Glob. Change Biol.* **2003**, *9*, 161–185. [[CrossRef](#)]

39. Smith, B.; Prentice, I.C.; Sykes, M.T. Representation of vegetation dynamics in the modelling of terrestrial ecosystems: Comparing two contrasting approaches within European climate space. *Glob. Ecol. Biogeogr.* **2001**, *10*, 621–637. [[CrossRef](#)]
40. Cassidy, A.E.; Christen, A.; Henry, G.H.R. Impacts of active retrogressive thaw slumps on vegetation, soil, and net ecosystem exchange of carbon dioxide in the Canadian High Arctic. *Arct. Sci.* **2017**, *3*, 179–202. [[CrossRef](#)]
41. Natali, S.M.; Watts, J.D.; Rogers, B.M.; Potter, S.; Ludwig, S.M.; Selbmann, A.-K.; Sullivan, P.F.; Abbott, B.W.; Arndt, K.A.; Birch, L.; et al. Large loss of CO₂ in winter observed across the northern permafrost region. *Nat. Clim. Change* **2019**, *9*, 852–857. [[CrossRef](#)]
42. Ueyama, M.; Iwata, H.; Harazono, Y.; Euskirchen, E.S.; Oechel, W.C.; Zona, D. Growing season and spatial variations of carbon fluxes of Arctic and boreal ecosystems in Alaska (USA). *Ecol. Appl.* **2013**, *23*, 1798–1816. [[CrossRef](#)]
43. Nanzad, L.; Zhang, J.H.; Batdelger, G.; Sharma, T.P.P.; Koju, U.A.; Wang, J.W.; Nabil, M. Analyzing NPP Response of Different Rangeland Types to Climatic Parameters over Mongolia. *Agronomy* **2021**, *11*, 647. [[CrossRef](#)]
44. Fisher, J.B.; Sikka, M.; Oechel, W.C.; Huntzinger, D.N.; Melton, J.R.; Koven, C.D.; Ahlstrom, A.; Arain, M.A.; Baker, I.; Chen, J.M.; et al. Carbon cycle uncertainty in the Alaskan Arctic. *Biogeosciences* **2014**, *11*, 4271–4288. [[CrossRef](#)]
45. Li, Z.-L.; Mu, C.-C.; Chen, X.; Wang, X.-Y.; Dong, W.-W.; Jia, L.; Mu, M.; Streletskaia, I.; Grebenets, V.; Sokratov, S.; et al. Changes in net ecosystem exchange of CO₂ in Arctic and their relationships with climate change during 2002–2017. *Adv. Clim. Change Res.* **2021**, *12*, 475–481. [[CrossRef](#)]
46. Commane, R.; Lindaas, J.; Benmergui, J.; Luus, K.A.; Chang, R.Y.; Daube, B.C.; Euskirchen, E.S.; Henderson, J.M.; Karion, A.; Miller, J.B. Carbon dioxide sources from Alaska driven by increasing early winter respiration from Arctic tundra. *Proc. Natl. Acad. Sci. USA* **2017**, *114*, 5361–5366. [[CrossRef](#)] [[PubMed](#)]
47. Miner, K.R.; Turetsky, M.R.; Malina, E.; Bartsch, A.; Tamminen, J.; McGuire, A.D.; Fix, A.; Sweeney, C.; Elder, C.D.; Miller, C.E. Permafrost carbon emissions in a changing Arctic. *Nat. Rev. Earth Environ.* **2022**, *3*, 55–67. [[CrossRef](#)]
48. Jenerette, G.D.; Scott, R.L.; Barron-Gafford, G.A.; Huxman, T.E. Gross primary production variability associated with meteorology, physiology, leaf area, and water supply in contrasting woodland and grassland semiarid riparian ecosystems. *J. Geophys. Res. Biogeosci.* **2009**, *114*, G04010. [[CrossRef](#)]
49. Pastick, N.J.; Jorgenson, M.T.; Goetz, S.J.; Jones, B.M.; Wylie, B.K.; Minsley, B.J.; Genet, H.; Knight, J.F.; Swanson, D.K.; Jorgenson, J.C. Spatiotemporal remote sensing of ecosystem change and causation across Alaska. *Glob. Change Biol.* **2019**, *25*, 1171–1189. [[CrossRef](#)] [[PubMed](#)]
50. Zha, J.R.; Zhuang, Q.L. Microbial decomposition processes and vulnerable arctic soil organic carbon in the 21st century. *Biogeosciences* **2018**, *15*, 5621–5634. [[CrossRef](#)]
51. May, J.L.; Healey, N.C.; Ahrends, H.E.; Hollister, R.D.; Tweedie, C.E.; Welker, J.M.; Gould, W.A.; Oberbauer, S.F. Short-Term Impacts of the Air Temperature on Greening and Senescence in Alaskan Arctic Plant Tundra Habitats. *Remote Sens.* **2017**, *9*, 1338. [[CrossRef](#)]
52. Dusenge, M.E.; Duarte, A.G.; Way, D.A. Plant carbon metabolism and climate change: Elevated CO₂ and temperature impacts on photosynthesis, photorespiration and respiration. *New Phytol.* **2019**, *221*, 32–49. [[CrossRef](#)]
53. Luus, K.A.; Lin, J.C.; Kelly, R.E.J.; Duguay, C.R. Subnivean Arctic and sub-Arctic net ecosystem exchange (NEE): Towards representing snow season processes in models of NEE using cryospheric remote sensing. *Prog. Phys. Geog.* **2013**, *37*, 484–515. [[CrossRef](#)]
54. Watts, J.D.; Natali, S.M.; Minions, C.; Risk, D.; Arndt, K.; Zona, D.; Euskirchen, E.S.; Rocha, A.V.; Sonnentag, O.; Helbig, M.; et al. Soil respiration strongly offsets carbon uptake in Alaska and Northwest Canada. *Environ. Res. Lett.* **2021**, *16*, 084051. [[CrossRef](#)]
55. Gougoulias, C.; Clark, J.M.; Shaw, L.J. The role of soil microbes in the global carbon cycle: Tracking the below-ground microbial processing of plant-derived carbon for manipulating carbon dynamics in agricultural systems. *J. Sci. Food Agric.* **2014**, *94*, 2362–2371. [[CrossRef](#)] [[PubMed](#)]
56. Siewert, M.B.; Hanisch, J.; Weiss, N.; Kuhry, P.; Maximov, T.C.; Hugelius, G. Comparing carbon storage of Siberian tundra and taiga permafrost ecosystems at very high spatial resolution. *J. Geophys. Res. Biogeosci.* **2015**, *120*, 1973–1994. [[CrossRef](#)]

Disclaimer/Publisher’s Note: The statements, opinions and data contained in all publications are solely those of the individual author(s) and contributor(s) and not of MDPI and/or the editor(s). MDPI and/or the editor(s) disclaim responsibility for any injury to people or property resulting from any ideas, methods, instructions or products referred to in the content.